UCRL-ID-125556

Intercomparison of the Seasonal Cycle in 200 hPa Kinetic Energy in AMIP GCM Simulations

J.S. Boyle

October 1996

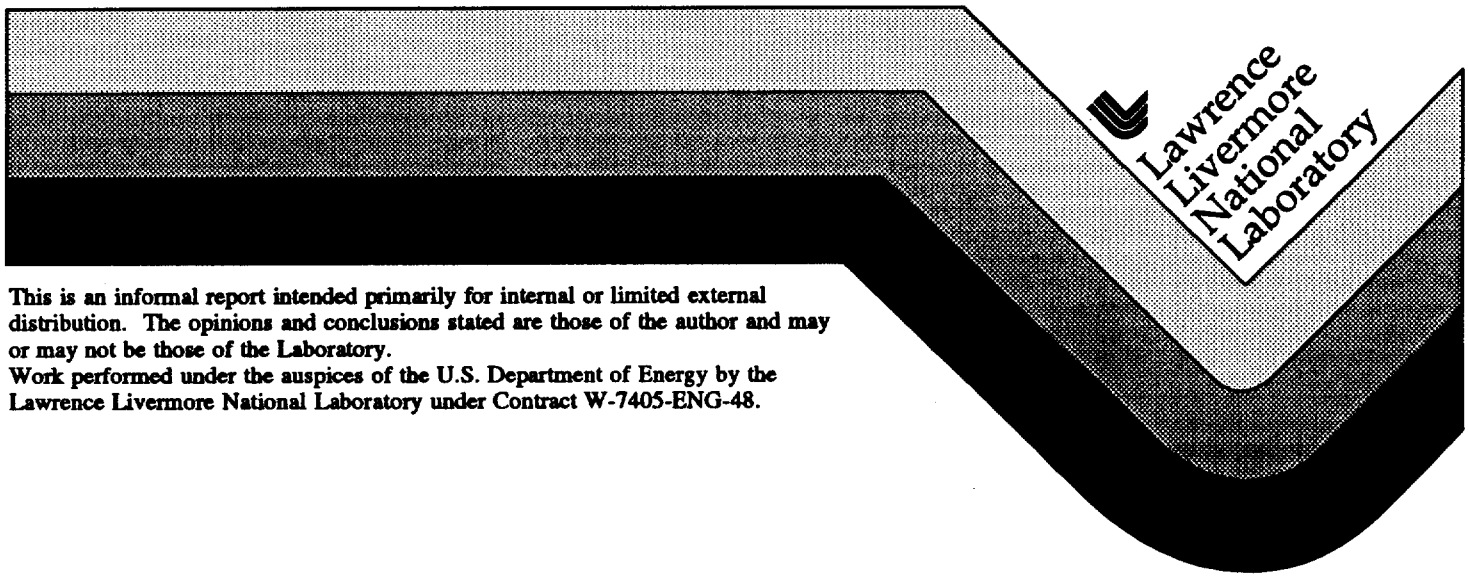

Intercomparison of the Seasonal Cycle in 200 hPa Kinetic Energy in AMIP GCM Simulations

James S. Boyle

Program for Climate Model Diagnosis and Intercomparison
Lawrence Livermore National Laboratory
Livermore, CA USA

October 1996

Abstract

The 200 hPa kinetic energy is represented by means of the spherical harmonic components for the AMIP simulations, the NCEP/NCAR reanalysis and the ECMWF reanalysis(ERA). The data used are the monthly mean wind fields for 1979 to 1988. The kinetic energy is decomposed into the divergent (DKE) and rotational (RKE) components and emphasis is placed on examining the former.

The two reanalysis data sets show reasonable agreement that is best for the rotational kinetic energy . The largest difference in the divergent kinetic energy occurs during the northern summer. As might be expected, the two analyses are closest in regions where there are sufficient observations such that the effects of the model used in the assimilation cycle are minimized.

The observed RKE shows only a slight seasonal cycle with a maximum occurring during the northern winter. The DKE, on the other hand, has a very pronounced seasonal cycle with maxima at the solsticial seasons and minima during the equinoctial seasons. The most energetic season is the northern summer (JJA), the least energetic the northern spring (MAM). SON is a transitional season with the three months having a large spread in values. The largest jump in DKE is seen from May to June, evidently in response to the onset of the Asian summer monsoon. The spectral decomposition of the DKE indicates that the NCEP analysis has more energy in the zonal component of the flow than the ERA. This is most pronounced during the northern summer.

The model results show a very large spread in the magnitudes of the RKE and DKE although the models all evince a seasonal variation in phase with that observed. The median value of the models systematically overestimates the observed RKE throughout the year and underestimates the DKE during the northern summer. These relations can be reversed for individual models. There is also a marked tendency for the models to have too much DKE in the zonal flow as compared to the reanalyses, especially at the higher energy levels. It does not appear possible to associate any specific model discrepancy with the particulars of the model formulation such as parameterizations or numerics at this level of analysis.

The median values of the seasonal cycle of RKE and DKE for the models are usually superior to those of any individual model. Results are also presented for simulations following the AMIP protocol but using updated versions of the original AMIP

entries. In most cases these new integrations show better agreement with the observations.

1. Introduction

In a previous work (Boyle, 1995) a study of the 200 hPa kinetic energy budgets of the AMIP simulation was undertaken. The kinetic energy was decomposed into the rotational and divergent components in terms of the spherical harmonics. In the present work the seasonal cycle of kinetic energy will be examined in more detail. In addition, the NCEP/NCAR (National Center for Environmental Prediction / National Center for Atmospheric Research) and ERA(European Centre for Medium Range Weather Forecast ReAnalysis) reanalyses fields will be used as verification data. These data were not available for the previous work.

The 30 models of AMIP have a wide variation in numerics, spatial resolution and physical parmeterizations. The goal of this work is to gain some insight into the nature of the model differences, and perhaps ambitiously, their causes. The divergent flow is intimately connected to the generation of kinetic energy by the secondary circulations and is closely linked with the diabatic forcing. In the tropics the divergent flow is directly coupled to the diabatic heating. In the Lorenz energetics framework the conversion from available potential energy to kinetic energy is accomplished by the divergent flow. Thus the DKE can be used as an indicator of the forcing by these processes as parameterized in the models. The effects of the various parameterization choices among the models considered is of prime interest. As will be shown the models exhibit a wide variation with respect to their representations of divergent kinetic energy. This is evidently the dynamical manifestation and integral of their physical parameterizations, and should provide a sensitive indicator of the models' mean state with respect to the observations.

The spherical harmonic decomposition has proved to be useful in past work. Lambert (1984, 1987) has performed a comprehensive analysis of observed data and output from the Canadian Climate Centre GCM (This model is an earlier version of the CCC model cited in this work.) He found that the model did a good job in qualitatively simulating the kinetic energy budget, but the magnitudes of some of the energies and conversions at some wavenumbers were not well represented in the simulation. The decomposition into spectral space will provide some measure of the scale dependency which might provide insight on the effects of the horizontal resolution of the models.

The intent here is not a contest to determine the "best" model. Rather, this work

should be seen as a summary of the state of atmospheric modeling from a rather narrow perspective. The results will show that a consensus among models has not been achieved and that more development is evidently required to simulate the atmospheric component of the climate system with complete fidelity.

2. Computational Formulation

In order to be clear in terminology, the equations for transforming to spherical harmonics will be presented. An arbitrary variable x distributed in latitude (ϕ) and longitude (λ) can be expressed in terms of spherical harmonics as follows:

$$x(\lambda, \phi) = \sum_{n=0}^{N} \sum_{m=-n}^{n} X_n^m P_n^m(\sin\phi) e^{im\lambda}$$

where

$$X_n^m = \frac{1}{2\pi} \int_0^{2\pi} x(\lambda, \phi) P_n^m(\sin\phi) \cos(\phi) e^{-im\lambda} d\phi d\lambda$$

and where P_n^m is the associated Legendre polynomial of the first kind of order m and degree n, X_n^m is a coefficient of the spherical harmonic representation of x, and N is the limiting wavenumber of the triangular truncation.

The question of the nature of the truncation arises when dealing with the representation of fields in terms of series of spherical harmonics. The models varied in their horizontal representations. Some were gridpoint models, while the rest used a spherical harmonic representation with either a triangular (T) or rhomboidal (R) truncation. In an attempt to be as even handed as possible for all the models, the calculations were carried out in the spherical harmonic space that is appropriate for each model. For the grid point models and the gridded observational data, a triangular truncation was chosen commensurate with the number of nodes from pole to pole. For the models cast in the spherical harmonics framework the calculations were carried out in the appropriate spectral space. The results are presented for regions of spectral space where any computational artifacts generated by these differences in representation and choices of truncation should be minimal.

Many of the results will be given in terms of the two dimensional wavenumber n. This method of presentation was originally advocated by Baer (1972) and has

proved useful in the work of Lambert(1984) and Boer and Shepherd(1983). In order to obtain results solely in terms of the two-dimensional wavenumber n, it is required to sum over the order m for each n.

3. Data

The Atmospheric Model Intercomparison Project (AMIP) of the World Climate Research Programme's Working Group on Numerical Experimentation (WGNE) permits some insight as to the general nature of the model GCM response to SST variations. The participants in AMIP simulate the global atmosphere for the decade 1979 to 1988 using a common solar constant and CO2 concentration, and a common monthly averaged SST and sea ice data set. An overview of AMIP is provided by Gates (1992).

The AMIP models used in this study are identified in Table 1 where their horizontal and vertical resolutions are shown. As important as the spatial configuration of the model are the parameterizations used to simulate processes such as moist convective heating, fluxes of heat, moisture and momentum, precipitation and clouds. The complete specifications of the parameterizations used in the models are described in Phillips (1994).

The observed data available were those of the operational analyses of the ECMWF, the NCEP/NCAR reanalysis and the ERA reanalysis. The ECMWF data were for the period 1980 to 1989. The shortcomings of the operational analyses of the ECMWF in regard to the divergent component of the wind are well documented (Trenberth and Olsen, 1988, 1988a; Lambert , 1989). The consensus of these studies is that the operational analysis had significant problems for the better part of the 1979 to 1988 decade. Nevertheless, the full 1980 to 1989 set of operational analyses were used here. This was done in order to calibrate the changes wrought by the reanalyses efforts, not with the intent of validating the models against these older data.

The reanalysis data used were chosen to be for the same period as the AMIP integrations. The reanalysis does not suffer from the inhomogeneity in assimilation systems of the operational products. It should be realized, however, that although the reanalysis uses a rather sophisticated variational analysis scheme, it still relies heavily upon the first guess generated by the 6 hour model forecast to produce the divergent component of the wind in data-sparse regions. It should also be kept in mind that the

database that supplies the analysis systems varies over the decade. The number, location and types of rawindsondes change, different types of remotely sensed data are introduced, and data from different platforms such as aircraft and buoys are phased in and out. The data from all the observed analyses were available on a 2.5 x 2.5 degree latitude-longitude grid.

4. Results

a. Global seasonal cycle in RKE and DKE

Figure 1 presents the seasonal cycle of the RKE and DKE for the three observed data sets used. Figure 1a, the RKE, shows a modest seasonal cycle, with a maximum during the northern winter, and a fairly flat curve through the rest of the year. There is a consistent underestimate of the rotational wind by the operational product with respect to the reanalyses. The bias is fairly constant throughout the year. The ERA values are higher than the NCEP/NCAR data from April to November, although differences in the two reanalysis are at most 10%.

Figure 1b shows the curves for the DKE. In contrast to the RKE, there is a very pronounced seasonal cycle in these data. There are maxima in the solstitial seasons, and minima in the equinoctial seasons. The lowest values are during the northern spring and the highest during the northern summer. The latter peak presumably is due to the Asian summer monsoon. As in the RKE, the operational analyses evince a consistent underestimate of the DKE throughout the year. However, the percentage error is much greater in the DKE case. In July there is more than a factor of two difference between the reanalyses and the operational product. This error is to be expected as documented by Trenberth and Olsen(1988) and Sardeshmukh (1993). The two re-analyses exhibit significant differences during the northern summer and fall. The difference is greatest in August, amounting to about 20% of the mean value.

b. Seasonal maps

Figure 1 provides a global overview of the character of the upper level flow and provides some quantitative estimates of the differences in the reanalyses. Some insight as to the causes of the differences can be obtained by examining charts of the seasonal means.

Figure 2a shows vectors of the NCEP DJF rotational winds and Fig. 2b shows the vectors of the difference of the ERA values minus the NCEP. Figure 2a displays

the familiar pattern of the DJF upper level winds, the field being dominated by the East Asian jet maximum. A similar plot of the ERA winds (not shown) is almost indistinguishable from the NCEP data using the scaling of Fig. 2a. The difference plot, Fig. 2b, reveals small but systematic differences in the reanalyses. As might be anticipated, the differences are largest in the tropics where the data are sparse and the dynamics of the models used in the data assimilation are more closely tied to the physical parameterizations. The differences in Fig. 2b depict coherent patterns, indicating that they are the result of systematic, not random, differences in the analyses. Although the percentage differences in the extratropics are small, the values in the Tropics are rather more substantial uncertainties, especially over the Indian Ocean and the eastern Pacific. The equatorial patterns are reminiscent of circulations forced by anomalous heating as shown by Gill (1982). The differences might be related to disparities in the heating generated by the two assimilation models.

Figure 3a shows the vectors of the NCEP DJF divergent winds and Fig. 3b shows the vectors of the difference of the ERA values minus those for the NCEP for DJF. Figure 3a depicts the conventional pattern of dominant action centers about the Maritime continent and South America. The divergence over the northern hemisphere stormtracks is also evident. Figure 3b indicates that the reanalyses have their major difference over the equatorial Western Pacific. In general, the differences are largest where the convective and thus divergent activity is larger and the data are sparse. This is predominantly in the equatorial regions.

Figure 4a is the same as Fig. 2a except for the northern summer (JJA). The broad region of strong upper level winds in the southern (winter) hemisphere is characteristic of this season. The difference patterns, Fig. 4b, are more widespread in the wintertime extratropics compared to DJF, Fig. 2b. These differences are likely a consequence of the sparse observations available in the southern hemisphere and the enhanced jet activity during the southern winter. This difference in the NCEP/NCAR and ERA reanalyses is also reflected in Fig. 1a.

Figure 5a shows the vectors of the NCEP JJA divergent winds and Fig. 5b shows the vectors of the difference of the ERA values minus those for the NCEP for JJA. The Asian monsoon is the dominant circulation feature in Fig. 5a. There are large differences, Fig. 5b, between the analyses all along the Equator, especially over the eastern Pacific. The largest discrepancies occur in the Eastern Pacific and not over the highly active Asian monsoon region. This might indicate that the observations can help to

constrain the divergent wind analyses to within fair agreement. In data sparse regions the disparate signatures of the assimilation systems become more evident.

c. KE in spectral space

As pointed out by Baer (1972), a useful plot is to contour the values of the spectral data in the space of m and n-m. This yields insight as to the important scales in the flow field. A plot of the NCEP divergent kinetic energy is presented in Fig. 6 for the JJA season. The values of n-m (the number of north-south nodes) are along the ordinate, while the zonal wavenumber m (the number of east-west nodes) form the abscissa. The point to be made from this figure is that almost all the power is contained in values that lie along the two axes. The contours levels in the figure are logarithmic; if linear contour levels are used then all the maxima are completely confined to the two axes. The rotational KE (not shown) is restricted almost exclusively to the m = 0 modes; the divergent KE tends to be more isotropic, with maxima along both the m = 0 and n-m = 0 axes. This difference is a reflection of the overwhelming dominance of the zonal wind in the rotational component. Baer (1972) displayed similar plots for the zonal and meridional KE, and these resemble the plots for the rotational and divergent KE, respectively.

The fact that most of the energy is distributed along the axes for the divergent KE suggests a way of reducing the complexity of the spectral decomposition by simply adding the modes along each axis and plotting the sums as a scatter diagram for all the models. This is appropriate only for the divergent KE since the RKE is entirely dominated by the m = 0 axis. For the divergent flow the m = 0 (no nodes along a line of constant latitude) modes can be interpreted as a Hadley / Ferrell north-south circulation. The n -m = 0 (no nodes along a line of constant longitude) represents an east-west or Walker type of flow.

Figure 7a is a Tukey sum/difference plot (Cleveland, 1985) of the NCEP DKE over the seasonal cycle.In these plots the ordinate displays the difference of the Σ[divergent KE (m- n=0)] - Σ[divergent KE (m = 0)] and the abscissa is the sum. The Tukey plot is designed to facilitate assessment of any biases in the data and their magnitudes. The energy levels along the abscissa are very nearly the same as those of the NCEP data in Fig. 1b since so much of the energy is confined to the axes. Figure 7a indicates that there is a tendency in the NCEP data to have a bias toward an east-west flow in the global divergent wind throughout the year, peaking in June. This fig-

ure also emphasizes some points also seen in Fig. 1b. The months of JJA stand apart as the most energetic, while the MAM months cluster at the low end. The biggest jump in energy occurs between May and June, with more than a twofold increase. The months of SON have the largest spread along the abscissa of any of the traditional seasons. This would indicate that, from this aspect of the data, this season is a transitional period and means derived from these months might be combining some disparate processes. The months of January and February are close, with December being closer to November.

Figure 7b is the same as Fig. 7a except for the ERA data. As indicated by Fig. 1, the ERA data are generally similar to the NCEP data. The ERA data exhibit a tendency for more north-south circulation than the NCEP data. In fact, for most of the year the points fall below the zero line of Fig. 7b. This indicates a more Hadley type of regime in the ERA assimilation. The same type of clustering among the seasons is seen in the ERA data. The JJA data are by themselves at high DKE, SON data are strung out along the abscissa, MAM data are a decided minima and DJF data are closer to MAM, with January and February being more similar than December. The differences in these figures suggest that the reanalyses have not yet entirely removed a component that is due to the individual assimilation system being used.

The purpose of presenting the reanalysis data was not give an exhaustive examination of the differences of the data, but to set the stage for model intercomparison. The reanalysis data provide a validation set that the models should closely resemble and the differences in the reanalyses indicates the upper limit of how close we can reasonably demand the models to be to any observed data. The next section will present the same type of analysis for the AMIP models.

5. Model Intercomparison

Figure 8a presents a statistical summary of the seasonal cycle in 200 hPa rotational kinetic energy for all the AMIP models. The differences amongst the models is substantial, the spread between the quartiles being about 50% of the observed value. The median value is fairly close to that observed but the lower quartile of the models is actually a better fit. The models as a whole overestimate the RKE. On the scale of this figure the two reanalyses are almost indistinguishable.

Figure 8b presents a statistical summary of the seasonal cycle in 200 hPa diver-

gent kinetic energy for all the AMIP models. The spread of the models is quite large. The median value tracks fairly well with the observed values with the exception of the northern summer. Over these months the analyses also disagree, but it appears that the models tend to underestimate the DKE even given this disagreement. The models also underestimate the sharpness of the jump in DKE in going from May to June.

To compliment the statistical summary of Fig. 8, the differences of the individual models from the NCEP analyses are presented in Figs. 9 and 11. These figures permit the examination of how a single model fits into the statistical portraits. These figures will be used as a starting point for some individual model comparisons. The same figures were produced using the ERA data (not shown). Since the results were virtually identical, only the NCEP figures will be presented. This indicates that the differences in the two reanalyses are somewhat less than the differences between the reanalyses and the individual models.

Figure 9 shows the differences in the 200 hPa RKE between the AMIP models and the NCEP reanalyses over the seasonal cycle. The RKE has only a slight seasonal cycle in the observations and the models do not show any pronounced cycle in their difference patterns over the year. The tendency for many models to overestimate the RKE is clear. Some models, e.g. YONU and IAP, display such poor climatologies that is was felt it would not be fruitful to examine them in detail. In the following the other models will be discussed.

There is no consistent and obvious relation between documented model properties and the extent of the differences seen in Fig. 9. One parameterization that is likely to be considered when discussing the upper level circulation is gravity wave drag. This parameterization has been documented to have an impact on the winds in GCMs. The models that do not have a GWD routine (CSU, DNM, GLA, GISS, IAP, SUNYA, UIUC, YONU) do not uniformly have large positive deviations in Fig. 9. However, the models with the largest positive deviations in Fig. 9 all come from this group and 8 of the 9 overestimate the RKE. There are models with GWD that also overestimate the RKE, however.

The tendency for GCMs to be too cold in the upper troposphere at the poles and too warm in the tropics (Boer et al. 1991) would be consistent with an excess of zonal geostrophic KE. Figure 10a shows the vector difference between the NCEP and CSU DJF 200 hPa winds. This model exhibits one of the larger positive deviations in Fig. 9. The figure indicates that this model has a consistent westerly anomaly with respect

to the NCEP. This is what would be expected from a cold pole bias. This model also does not have a GWD routine. Note however, that there is a spatial structure to the difference pattern in Fig. 10a. There is a definite connection to topographical features and the location of local jet maxima. All the model difference fields have this character. The point is that the model error is not uniform nor random, but is due to systematic shifts in the positions and intensities of climatological features in the wind field. Thus the problem is deeper than the simple bias consistent with Fig. 9, although eliminating any such bias is without doubt a desirable goal. Figure 10b displays the difference between the NCEP DKE and the COLA DJF rotational wind. This is one of the models that showed an underestimate of the RKE. Again there are coherent patterns to the difference fields indicating some systematic errors. Looking at such difference patterns from all the models (not shown), it is difficult to generalize the error. There are some preferred regions where errors are large, such as jet exit regions, but there is enough individuality to make sweeping statements difficult. The difference field between the two reanalyses, Fig. 2a, shows the largest discrepancies in the regions where there are little data, mostly in the tropics. The differences of the models from the NCEP tend to occur in the active regions of the midlatitude jets as well as the tropics, but the models display large discrepancies in regions where the two reanalyses are in agreement.

Figure 11 shows the differences in the 200 hPa DKE between the AMIP models and the NCEP reanalyses over the seasonal cycle. The DKE has a substantial seasonal cycle and the models exhibit more seasonal variation about the observations than in the RKE. As in the figure for the RKE, this figure was redrawn using the ERA data and the result was virtually identical to Fig. 11. Most of the models strongly underestimate the DKE during the northern summer, but a few err in the opposite direction.

Figure 12a shows the vector difference of the divergent wind between selected models and NCEP at 200 hPa for the JJA season. Figure 12a is for the GLA model which overestimates the DKE in Fig. 11. The most striking differences occur in tropical, convectively active regions, although there are non-negligible values in mid-latitudes and near the poles. Figure 12b shows the results for the COLA model, which was one of the many that underestimated the JJA DKE in Fig. 11. From about the Greenwich meridian eastward to 120E, the differences in the GLA and COLA models are opposite, which could be interpreted as indicating that the GLA model overestimates the outflow from the summer monsoon and the COLA model does not produce

enough. But this type of error does not appear to be uniformly true about the globe. Over tropical South America the patterns of the two models are similar, and they imply that the models are overestimating the divergence. The SPCZ is prominent in Fig. 12a, and the tropical east Pacific from 150W to 110W is prominent in Fig. 12b. These active regions also are seen in the plots from all the other models, although the nature of the difference varies from model to model as it does in Fig. 12. The difference plots between the two reanalyses, Fig. 3a, also show the largest differences in the convectivley active regions not dissimilar to the differences in the model and NCEP data. The active regions, of the DKE occur in the tropics where the sparse observations do not allow for an unambiguous analysis. The differences between the two reanalyses could be chiefly due to the models used in the data assimilation.

Figure 13a presents the data for the GLA model as in Fig. 7. The enhanced energy levels in JJA season compared to the observations are apparent. Qualitatively, the seasonal cycle is like the reanalysis. The JJA months are at high energy levels, the SON is a transition season, and the MAM is a minimum point in Fig. 13a. The months with the greatest DKE tend to go up along the ordinate. This a consistent behavior across a majority of the models in that at higher levels of DKE there is a tendency to put proportionately more DKE into the east-west modes.

Figure 13b is for the BMRC model. This model is shown since it displays a characteristic common to a number of models, namely that there is an almost linear relation between the total DKE and the bias towards zonal circulation. This is the most systematic behavior that can be identified using these data. Note that the total DKE is comparable to the observations, but the details of the spectral distribution is quite different, especially during the northern winter. Figure 13 is for the COLA model. This model consistently underestimates the DKE and the seasonal cycle is confined to a rather small energy range. This model and the GLA, Fig. 13a, show the largest range in the characteristics of the DKE.

6. Discussion and Conclusions

The AMIP was intended to document the state of AGCM modeling and to facilitate diagnosis of the causes of any differences that showed themselves. The models do display a number of large differences, but it is not a trivial task to figure out the causes of these. For example, the tendency of the models to have poles which are too cold

and a tropical region which is too warm has been documented for some time (Boer et al. , 1991), but there has not been any fundamental flaw uncovered which explains this error.

In this discussion, the utility of the DKE as a model diagnostic will be examined. The DKE is closely tied to many of the fundamental physical processes that the models are attempting to simulate. Thus, the DKE may be a sensitive indicator of how well the model parameterizations are emulating nature. A difficulty with this field is that its actual value has been rather poorly known. The reanalysis efforts at NCEP and ECMWF produce a more reliable and consistent divergent wind record than was previously available. It must be recognized that the divergent wind represents only about 10% of the global KE and thus the uncertainty in the measurements is still significant and the model used in the data assimilation may project a signal of its own onto the analysis. Some evidence for this has been presented in previous sections of this work. The seasonal comparison of the NCEP and ERA DKE, Figs. 1 and 7, paints a picture of reasonable agreement. These figures will form a backdrop for some of the individual model results. It is also anticipated that the data on these figures place a strong constraint on the circulation expected from the simulations. What is shown is not only the global RKE and DKE but also some crucial aspects of their spectral decomposition, and the most basic temporal decomposition into the seasonal cycle. This is done for ten years of simulation and observations. It would seem that if the models are producing a correct simulation of the dynamics of the atmosphere, then they must closely resemble these observations, and it would seem highly unlikely that the models could produce a similar behavior unless the essentials of the physics were modeled successfully.

The ECMWF and UGAMP models form an interesting pair since essentially the only difference between them is in the convective parameterization used. ECMWF used the mass flux scheme of Tiedtke while UGAMP used the adjustment technique of Betts-Miller. Thus these two simulations provide some measure of how sensitive the DKE is to a particular parameterization. Figures 14a and 14b present a comparison of the UGAMP and ECMWF models for the seasonal cycle in DKE. The DKE energy levels are comparable, but the distribution between the zonal and meridional flow is markedly different. In this case the ECMWF compares favorably with the observations, but the UGAMP DKE is distinctly more Hadley in nature than is observed. The difference is so dramatic that the anomalous Hadley circulation near the

Equator is obvious in vector plots of the divergent wind (Boyle, 1995). As might be expected the DKE is sensitive to the convective parameterization. This would seem to indicate that the Betts-Miller scheme needs additional tuning in the UGAMP model.

The UCLA and CSU models, Figs. 14c and 14d, are close cousins in that the CSU model was originally derived from an earlier version of the UCLA code. This kinship is evident in the figures. They also resemble each other in the RKE, Fig. 9. Both somewhat underestimate the DKE, but do have a seasonal cycle similar to the reanalyses in the limited DKE values they encompass. CSU does not have a GWD parameterization but this does not appear to have a dramatic impact on the DKE. The CSU and UCLA models differ in many ways but both use the Arakawa-Schubert penetrative convection scheme, and the UGAMP and ECMWF differ in only the convective parameterization used. This is evidence of the almost overwhelming sensitivity of models to this critical aspect of the simulations.

Figure 13a shows the results from the GLA simulation. This is one of the most energetic models in terms of DKE. This is seen on the long timescales studied here and also on the intra-seasonal time scale considered by Slingo et al. (1996).They identified the GLA model as one of the better simulations of the intraseasonal(Madden-Julian) oscillation, although none of the models did very well in simulating the MJO. The months in Fig. 13a have roughly similar placement with respect to each other as do the observations, but at a greatly elevated DKE level. The DKE is almost a factor of two greater during the northern summer than in the observations. Slingo et al. (1996) also identified the UKMO model as one of the better simulations of the MJO, and it too has rather elevated DKE levels with respect to the reanalyses. Both of these models, GLA and UKMO, have a larger proportion of DKE in the east-west circulation than seen in the reanalyses.

Since the original AMIP experiment some modeling groups have run new versions of their models using the AMIP protocols. The results from these integrations can be used as another measure of the sensitivity and utility of the DKE as a diagnostic. In these subsequent runs there can be a modest or substantial revamping of some parameterizations. Figures 15 and 16 are the seasonal comparisons of these subsequent runs for the RKE and DKE, respectively. In some models the two figures are almost identical. The only change in the two MRI simulations was the inclusion of a GWD parameterization in the second run. For the data displayed here, this had a negligible impact. Three models, LMD, MPI and NRL, largely removed the underesti-

mate in DKE during the northern warm months and in some cases reversed the sign of this difference from Fig. 11. LMD seems to have done this at the expense of slightly overestimating the DKE in the northern cold months. The CNRM model underwent very substantial revision, and this is reflected in some large shifts in the DKE.

Figures 17a and 17b are the DKE seasonal Tukey diagrams for the NRL original and revised run. The original, Fig. 17a, has the same type of structure seen in the BMRC figure(Fig. 13b), in that at higher levels of DKE the values move up along the ordinate, indicating too much east-west flow. In the second run, Fig. 17b, the slope of this bias is slightly decreased but the northern summer levels go from an underestimate to an overestimate with respect to reanalysis. The relative positions of the months remain approximately the same in the two runs, although the September value has improved. The NRL model appears to retain a slight east-west bias.

Figures 17c and 17d are the DKE seasonal Tukey diagrams for the MPI simulations. The MPI revisit has improved the DKE while slightly increasing the bias with respect to the NCEP RKE values. The changes made by MPI, Fig. 17d, were such that the model DKE seasonal cycle closely agrees with the reanalysis; indeed, given the uncertainty in this field, the MPI might well be as good as one can expect at this stage of knowledge.

This study shows that the DKE and RKE can be useful in identifying some model differences. The models generally overestimate the RKE and underestimate the DKE, the latter especially so during the boreal summer. There is an appreciable spread in the values of both the DKE and RKE. The seasonal variation of these quantities are well simulated, but the magnitude and details of the circulation structure differ substantially in some simulations.

Acknowledgments. The cooperation of the ECMWF in making their forecast model available and in providing expert technical advice for this research is gratefully acknowledged. The generosity of the modeling groups involved in AMIP in making their results available is greatly appreciated. This work was performed under the auspices of the Department of Energy Environmental Sciences Division by the Lawrence Livermore National Laboratory under contract W-7405-ENG-48.

7. References

Baer, F., 1972: An alternate scale representation of atmospheric energy spectra. *J. Atmos. Sci.*, **29**, 649-664.

Boer, G. J. and T. G. Shepherd, 1983: Large-scale two-dimensional turbulence in the atmosphere. *J. Atmos. Sci.*, **40**, 164-184.

Boer, G. J., K. Arpe, M. Blackburn, M. Deque, W. L. Gates, T. L. Hart, H. Le Treut, E. Roeckner, D. A. Sheinin, I., Simmonds, R. N. B. Smith, T. Tokioka, R. T. Wetherald, and D. Williamson, 1991: An Intercomparison of the Climates Simulated by 14 Atmospheric General Circulation Models, WRCP - 58, WMO/TD - No. 425, World Meteorolgical Organization, Geneva.

Boyle, J. S., 1995: Intercomparison of the spectral characteristics of the 200 hPa kinetic energy in AMIP GCM simulations. PCMDI Report No. 23, UCRL-ID-121413, Lawrence Livermore National Laboratory, Unviersity of California, 39pp.

Cleveland, W. S., 1985 : *The Elements of Graphing Data*, Wadsworth Advanced Books and Software, Monterey, CA, 323pp

Gates, W. L., 1992: AMIP : The atmospheric model intercomparison project. *Bull. Amer. Meteor. Soc.*, 73, 1962-1970.

Gill, A. E., 1982: *Atmosphere-Ocean Dynamics*, Academic Press, New York, 662pp.

Lambert, S. J., 1984: A global available potential energy-kinetic energy budget in terms of the two-dimensional wavenumber for the FGGE year. *Atmos.-Ocean*, **22**, 265-282.

Lambert, S. J., 1987: Spectral energetics of the Canadian Climate Centre general circulation model., *Mon. Wea. Rev.*, **115,** 1295-1304.

Lambert, S. J., 1989: A comparison of divergent winds from the National Meteorological Center and the European Centre for Medium Range Weather Forecasts global analyses for 1980-1986. *Mon. Wea. Rev.*, **117,** 995-1001.

Lambert, S. J., 1990: Observed and simulated intraseasonal energetics. *J. Clim.*, **3**, 1330-1346.

Phillips, T. J., 1994: A summary documentation of the AMIP models. PCMDI Report No. 18, Program for Climate Model Diagnosis and Intercomparison, University of California, Lawrence Livermore National Laboratory, Livermore, CA, 343pp.

Sardeshmukh, P. D., 1993: The baroclinic chi problem and its application to the diag-

nosis of atmospheric heating rates., *J. Atmos. Sci.*, **50**, 1099-1112.

Slingo, J. M. et al., 1996: Intraseasonal oscillations in 15 atmospheric general circulation models: results from an AMIP diagnostic subproject. *Climate Dynamics*, **12,** 325-357.

Tiedtke, M., 1989: A comprehensive mass flux scheme for cumulus parameterization in large scale models., *Mon. Wea. Rev.*, **117**, 1779-1800.

Trenberth, K. E. and J. G. Olson, 1988: *Evaluation of NMC Global Analysis: 1979-1987*. NCAR/TN-299+STR, Climate and Global Dynamics Division, NCAR, Boulder, CO 82pp.

Trenberth, K. E., and J. G. Olsen, 1988a: *A Comparison between NMC and ECMWF global analyses: 1980-1986.* NCAR/TN-301+STR,Climate and Global Dynamics Division, NCAR, Boulder, CO 96pp.

AMIP Model	Horizontal		Vertical		
	Representation	Resolution	Coordinates	No. Levels	Bottom, Top
BMRC	spectral	rhomboidal 31	sigma	9 (3, 3)	991, 9 hPa
CCC	spectral	triangular 32	hybrid	10 (3, 4)	980, 5 hPa
CNRM	spectral	triangular 42	hybrid	30 (4, 20)	995, 0.01 hPa
COLA	spectral	rhomboidal 40	sigma	18 (5, 4)	995, 10 hPa
CSIRO	spectral	rhomboidal 21	sigma	9 (3, 3)	979, 21 hPa
CSU	finite difference	4 x 5 degrees	modified sigma	17 (2, 6)	variable, 51 hPa
DERF	spectral	triangular 42	sigma	18 (5, 5)	998, 2 hPa
DNM	finite difference	4 x 5 degrees	sigma	7 (1, 1)	929, 71 hPa
ECMWF	spectral	triangular 42	hybrid	19 (5, 7)	996, 10 hPa
GFDL	spectral	rhomboidal 30	sigma	14 (4, 4)	997, 15 hPa
GISS	finite difference	4 x 5 degrees	sigma	9 (2, 2)	975, 10 hPa
GLA	finite difference	4 x 5 degrees	sigma	17 (5, 4)	994, 12 hPa
GSFC	finite difference	4 x 5 degrees	sigma	20 (5, 7)	994, 10 hPa
IAP	finite difference	4 x 5 degrees	modified sigma	2 (0, 0)	800, 200 hPa
JMA	spectral	triangular 42	hybrid	21 (6, 7)	995, 10 hPa
LMD	finite difference	50 sinlat x 64 lon	sigma	11 (3, 2)	979, 4 hPa
MGO	spectral	triangular 30	sigma	14 (5, 4)	992, 13 hPa
MPI	spectral	triangular 42	hybrid	19 (5, 7)	996, 10 hPa
MRI	finite difference	4 x 5 degrees	hybrid	15 (1, 9)	variable, 1 hPa
NCAR	spectral	triangular 42	hybrid	18 (4, 7)	992, 3 hPa
NMC	spectral	triangular 40	sigma	18 (5, 4)	995, 21 hPa
NRL	spectral	triangular 47	hybrid	18 (5, 5)	995, 1 hPa
RPN	spectral semi-Lagrangian	triangular 63	sigma	23 (7, 7)	1000, 10 hPa
SUNYA	spectral	rhomboidal 15	sigma	12 (3, 5)	991, 9 hPa
SUNYA/NCAR	spectral	triangular 31	hybrid/sigma	18 (4, 7)	993, 5 hPa
UCLA	finite difference	4 x 5 degrees	modified sigma	15 (2, 9)	variable, 1 hPa
UGAMP	spectral	triangular 42	hybrid	19 (5, 7)	996, 10 hPa
UIUC	finite difference	4 x 5 degrees	sigma	7 (3, 0)	990, 200 hPa
UKMO	finite difference	2.5 x 3.75 degrees	hybrid	19 (4, 7)	997, 5 hPa
YONU	finite difference	4 x 5 degrees	modified sigma	5 (1, 1)	900, 100 hPa

Table 1. The AMIP models used in this study and some aspects of their spatial resolution. Table taken from Phillips (1994).

Number in Figs. 15 and 16	AMIP run	Modeling Group
1	original	CNRM
2	revision	
3	original	COLA
4	revison	
5	original	LMD
6	revision	
7	original	MPI
8	revision	
9	original	MRI
10	revision	
11	original	NRL
12	revision	
13	original	SUNY/NCAR
14	revision	
15	original	YONU
16	revision	

Table 2. List of original and revised AMIP simulations used in Fig. 15.

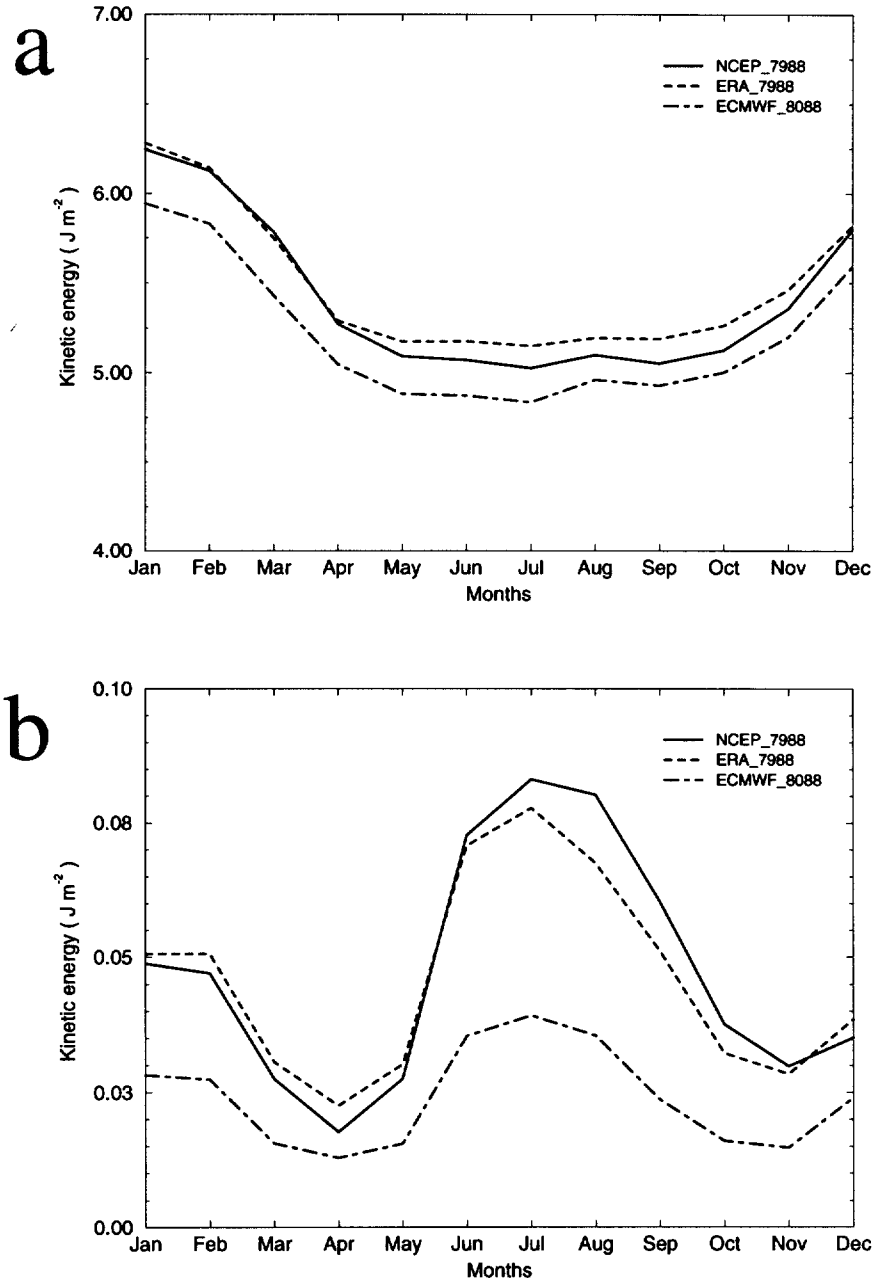

Figure 1.(a) Seasonal cycle of rotational kinetic energy (RKE) at 200 hPa for the NCEP / NCAR reanalyses, the ECMWF reanalyses(ERA), and the operational ECMWF analyses for the period 1979 to 1988. (b) As in (a) except for the divergent kinetic energy (DKE).

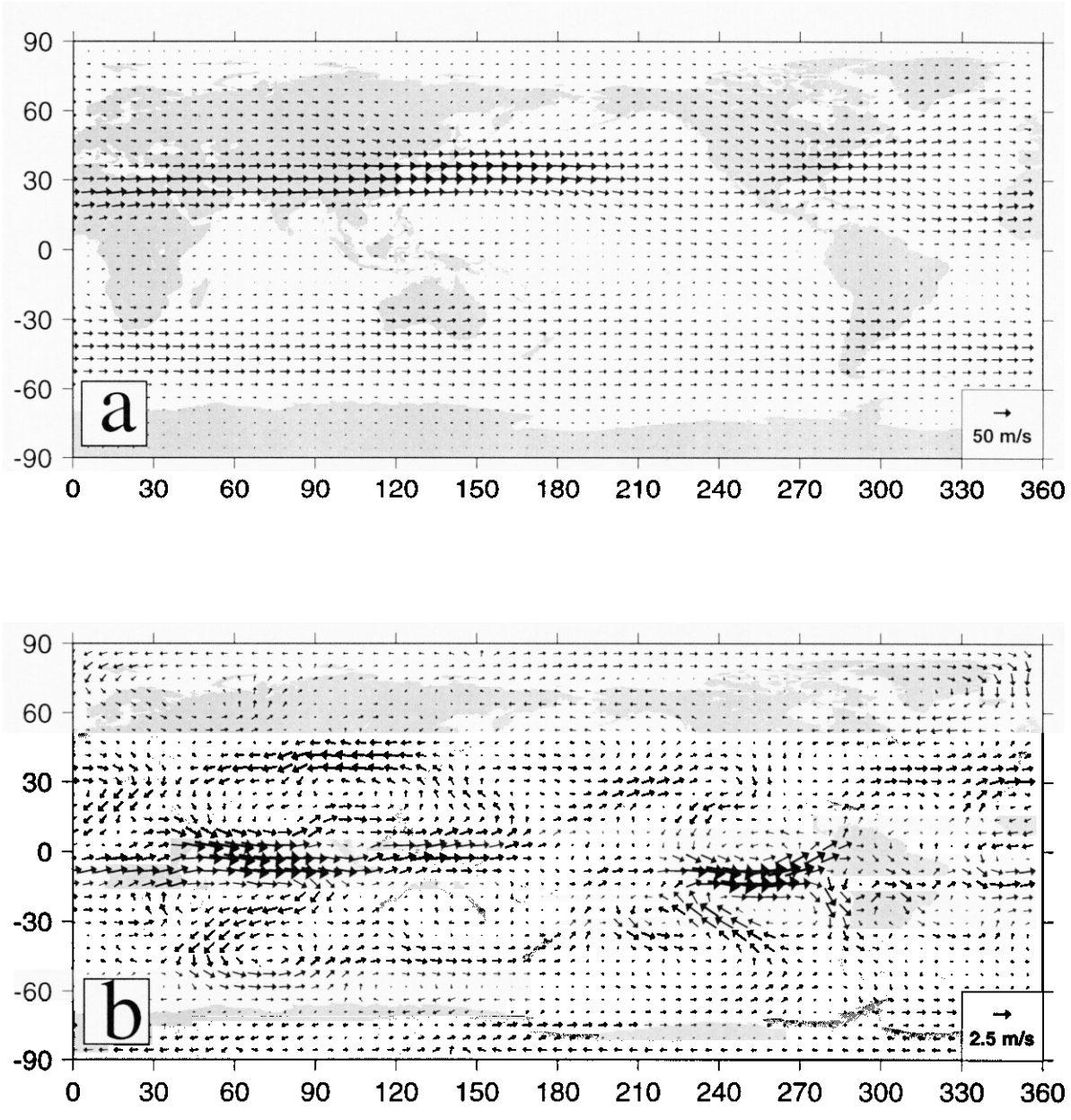

Figure 2. (a) The mean rotational wind for the NCEP / NCAR reanalysis for the northern winter (December, January, February) for the period 1979 to 1988.
(b) The difference between the mean rotational wind of the ECMWF reanalysis(ERA) minus the NCEP / NCAR reanalysis for the northern winter (December, January, February) for the period 1979 to 1988. Note the difference in scale between (a) and (b).

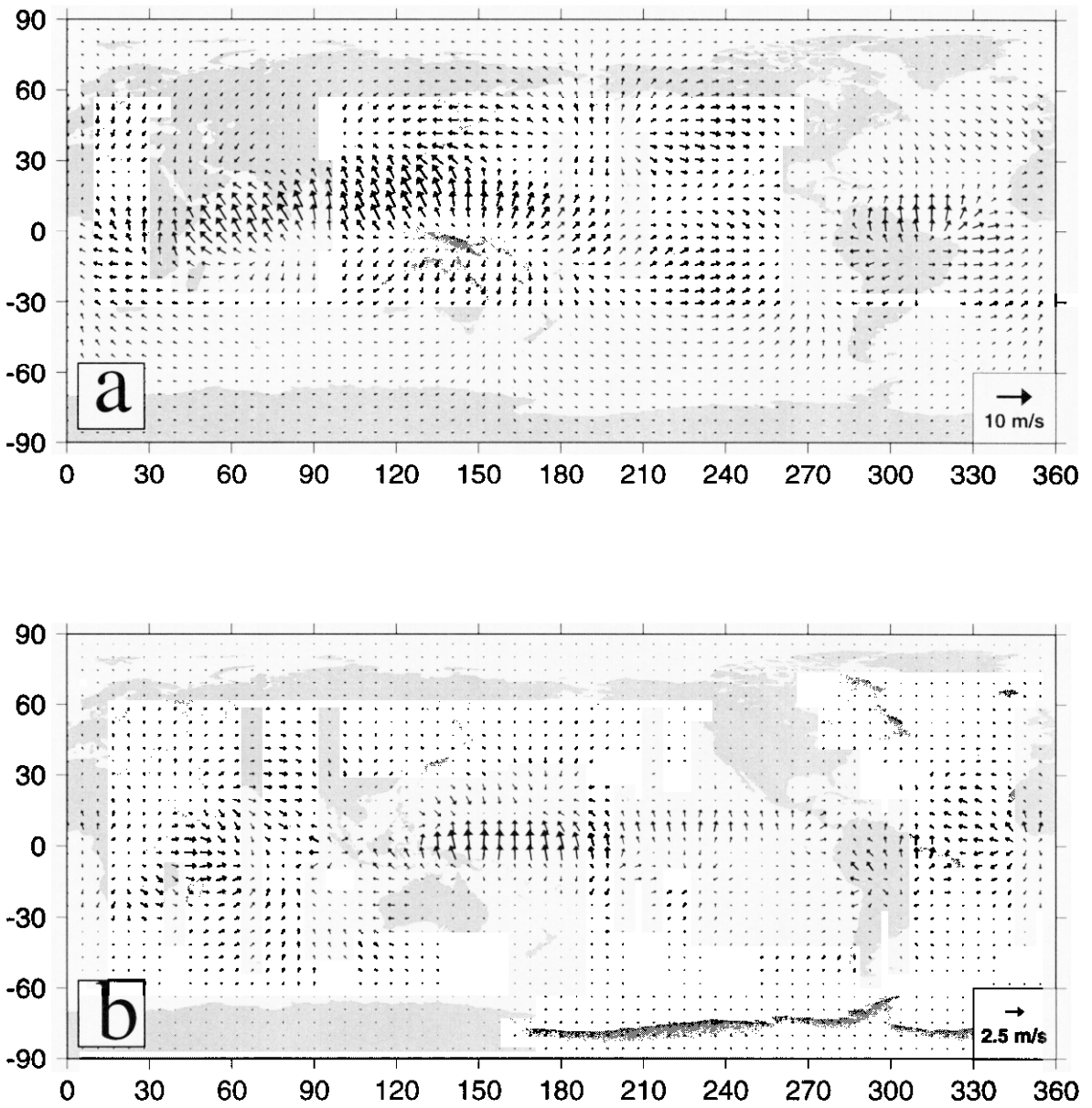

Figure 3. (a) The mean divergent wind for the NCEP / NCAR reanalysis for the northern winter (December, January, February) for the period 1979 to 1988.
(b) The difference between the divergent wind of the ECMWF reanalysis(ERA) minus the NCEP / NCAR reanalysis for the northern winter (December, January, February) for the period 1979 to 1988. Note the difference in scale between (a) and (b).

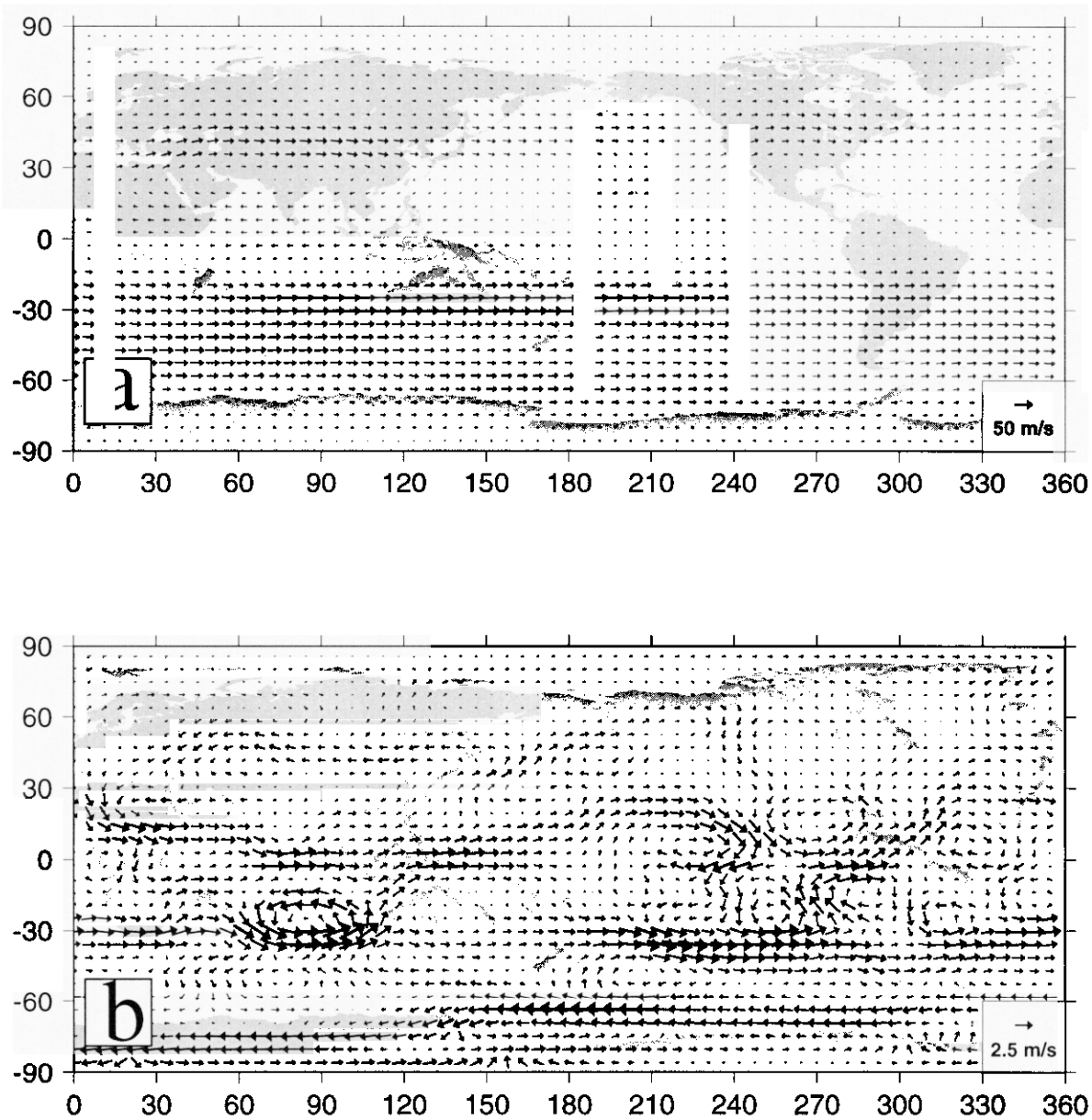

Figure 4. (a) The mean rotational wind for the NCEP / NCAR reanalysis for the northern summer (June, July, August) for the period 1979 to 1988.
(b) The difference between the mean rotational wind of the ECMWF reanalysis(ERA) minus the NCEP / NCAR reanalysis for the northern summer (June, July, August) for the period 1979 to 1988.
Note the difference in scale between (a) and (b).

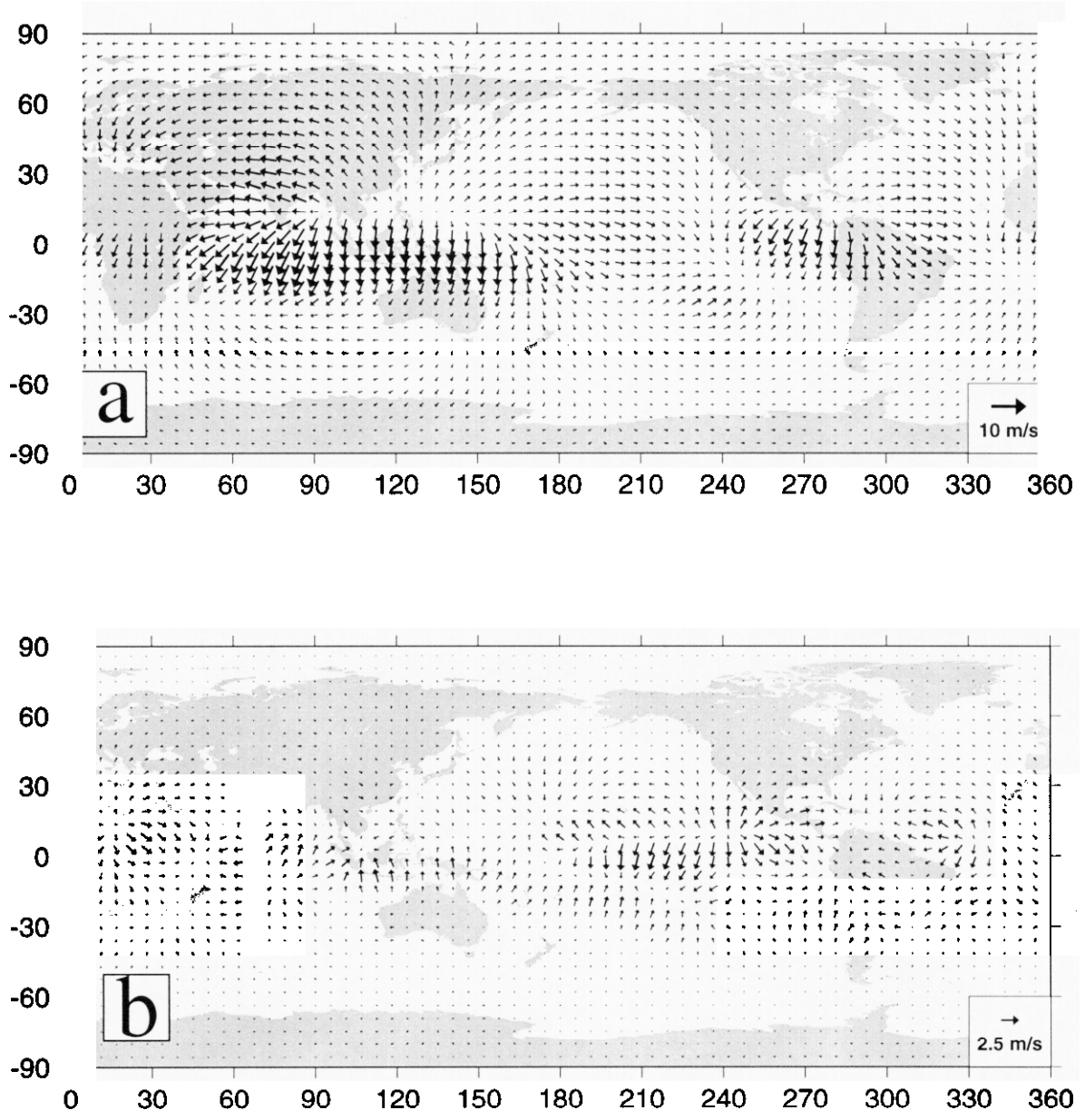

Figure 5. (a) The mean divergent wind for the NCEP / NCAR reanalysis for the northern summer (June, July, August) for the period 1979 to 1988.
(b) The difference between the divergent wind of the ECMWF reanalysis(ERA) minus the NCEP / NCAR reanalysis, for the northern summer (June, July, August) for the period 1979 to 1988.
Note the difference in scale between (a) and (b).

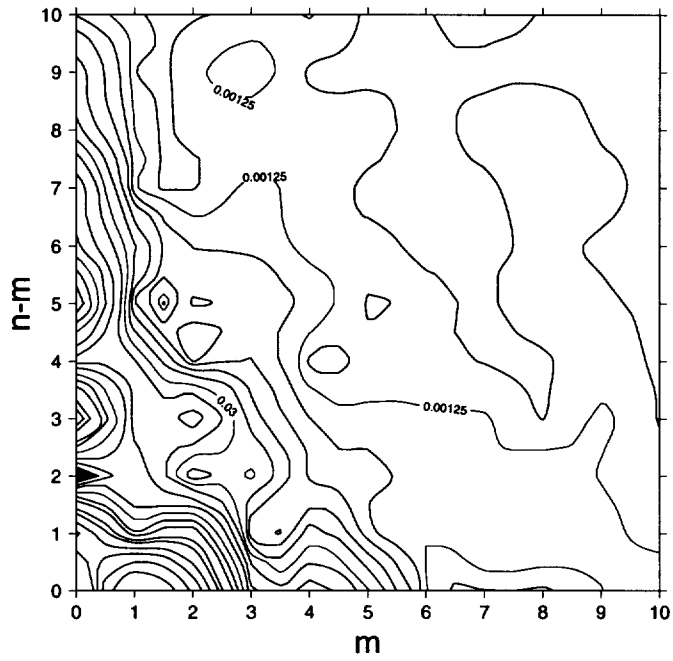

Figure 6. The divergent kinetic energy of the NCEP / NCAR reanalysis for northern summer (June, July, August) for the period 1979 to 1988 in the spectral space of the spherical harmonics. The ordinate is the n-m modes which represent the number of north-south nodes, the abscissa is the number of east-west nodes. The contours are on a logarithmic scale. Units are in Jm^{-2}.

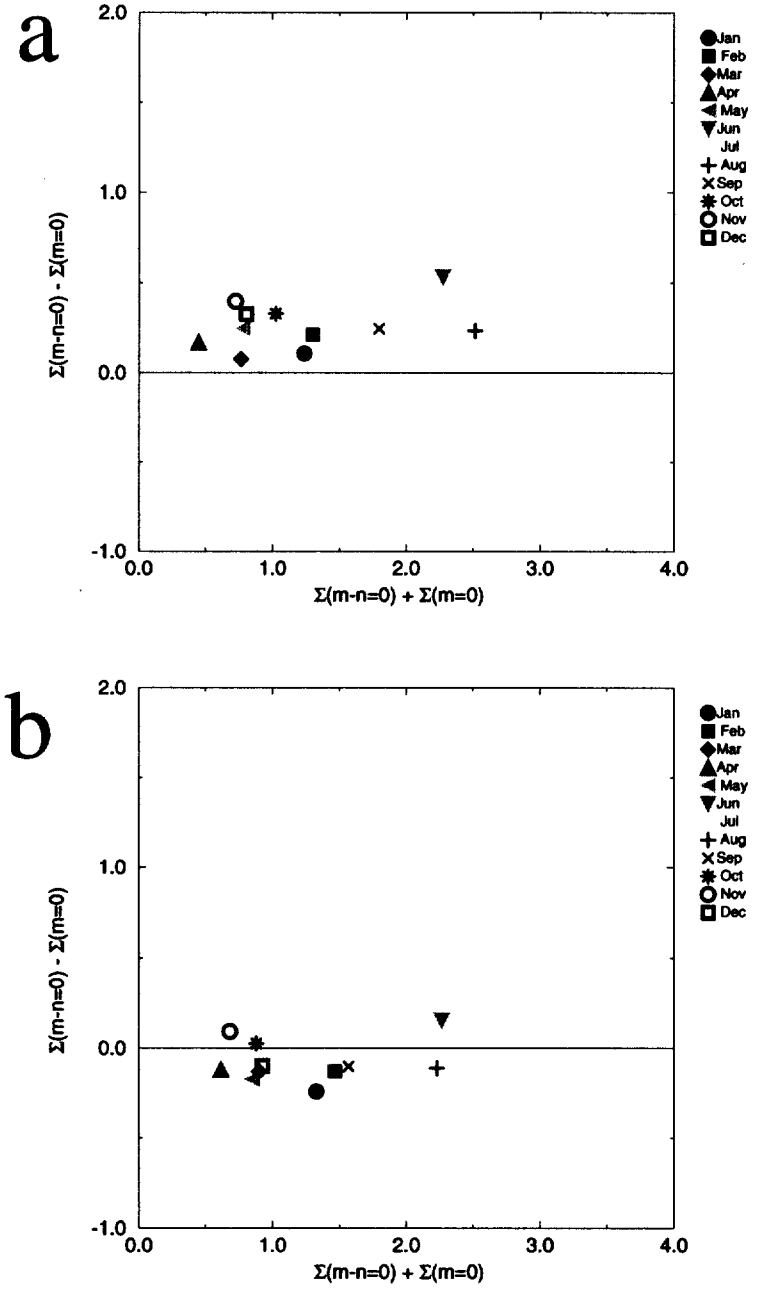

Figure 7. (a) A Tukey sum-difference plot for the $\Sigma(m=0)$ and $\Sigma(n-m=0)$ modes of the 200 hPa divergent kinetic energy for the seasonal cycle of the NCEP / NCAR reanalyses.
(b) As in (a) except for the ECMWF reanalyses(ERA).

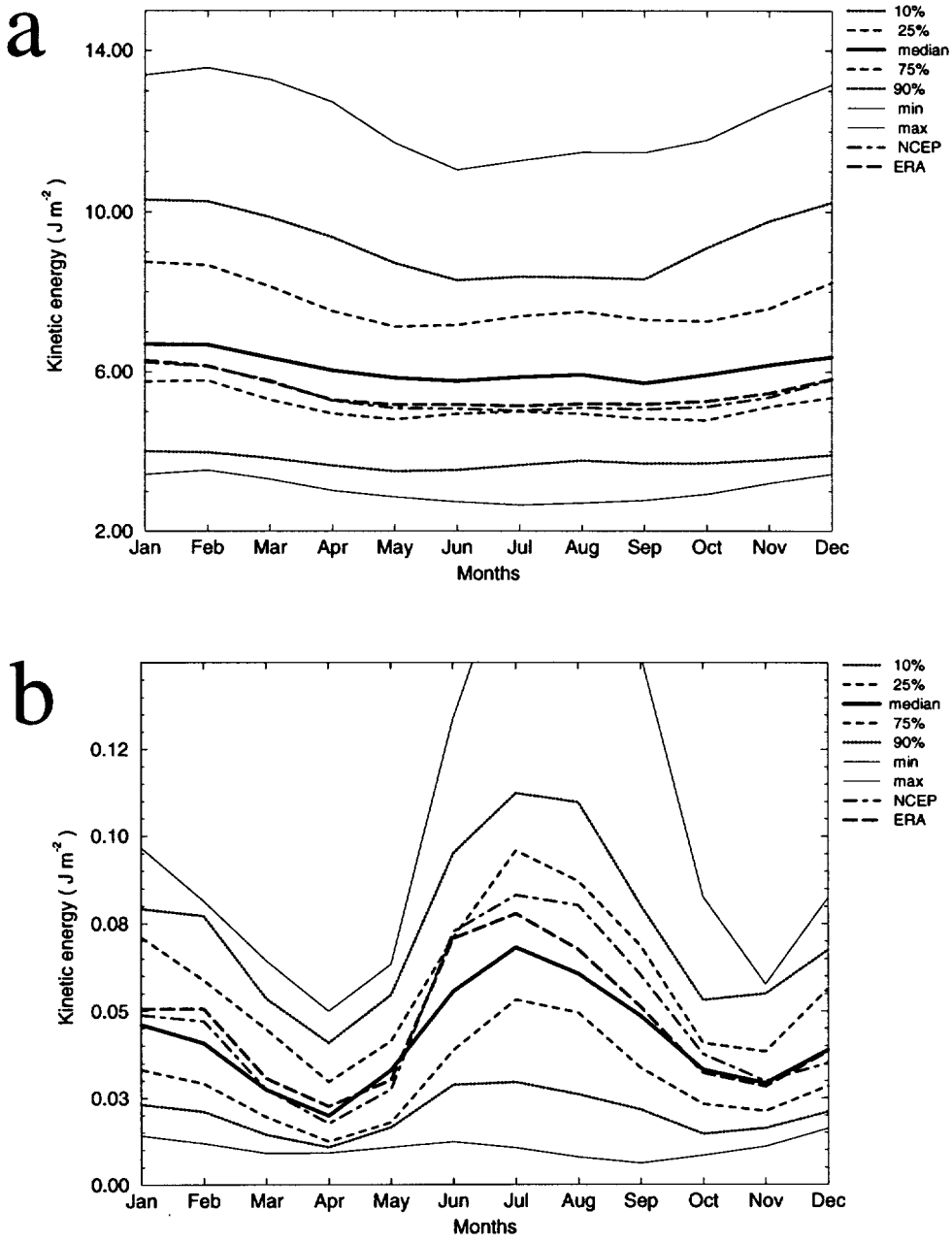

Figure 8.(a) Statistical summary of the seasonal cycle of rotational kinetic energy (RKE) at 200 hPa for all the AMIP models for the period 1979 to 1988. The NCEP / NCAR reanalyses and the ECMWF reanalyses(ERA) are also plotted for reference.
(b) As in (a) except for the divergent kinetic energy (DKE).

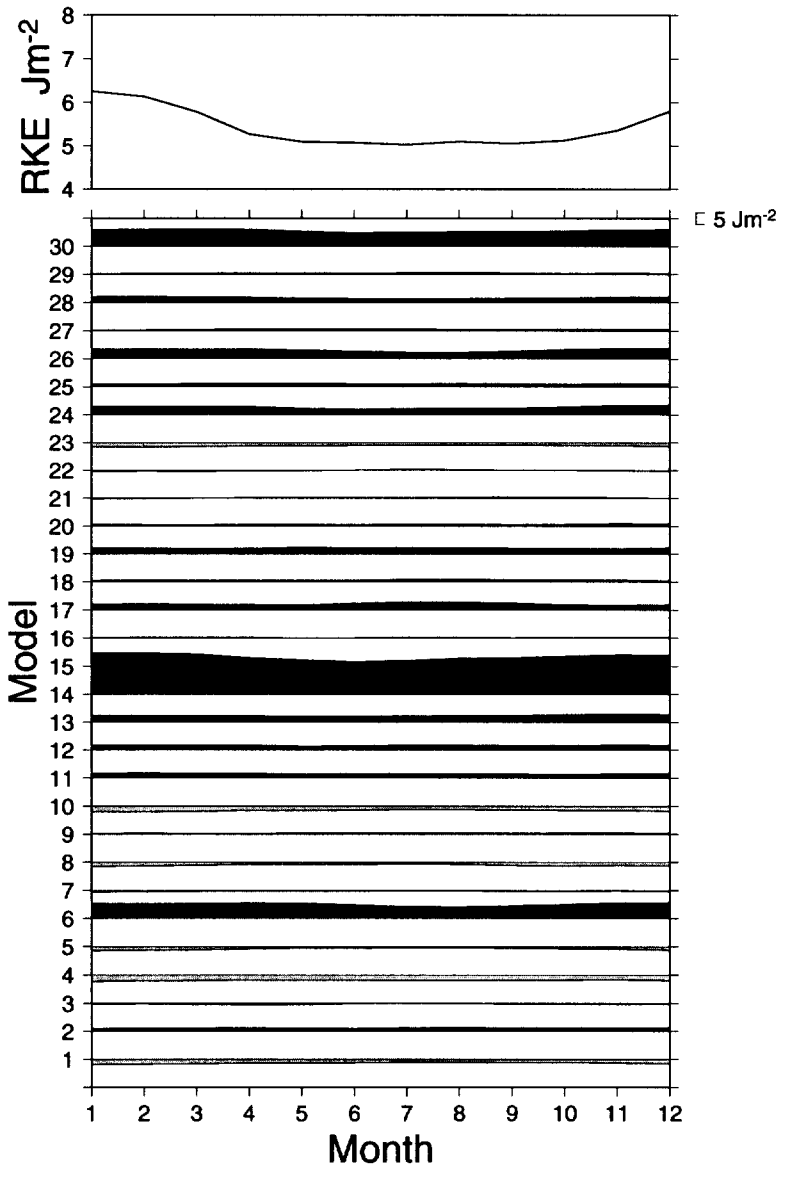

Figure 9. The seasonal cycle of the difference in 200 hPa RKE between the AMIP models and the NCEP / NCAR reanalyses. The dark shading represents an overestimate, the light shading indicates an underestimate by the model. The models are ordered alphabetically (BMRC = 1) as in Table 1. The curve at top are the NCEP / NCAR reanalyses values used in the difference.

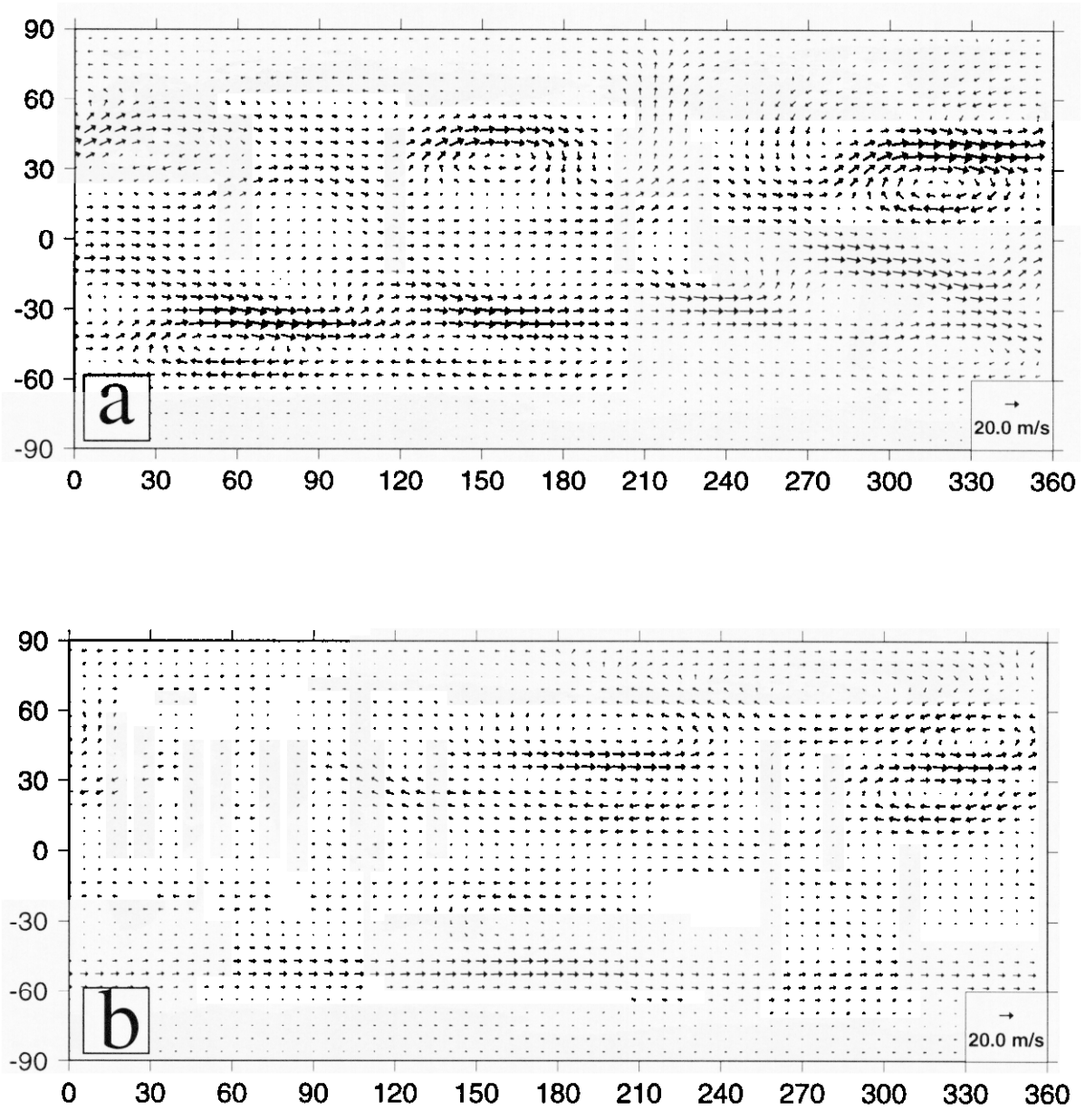

Figure 10. (a) The difference between the rotational wind of the CSU simulation minus the NCEP / NCAR reanalyses for the northern winter (December, January, February) for the period 1979 to 1988. (b) As in (a) except for the COLA model.

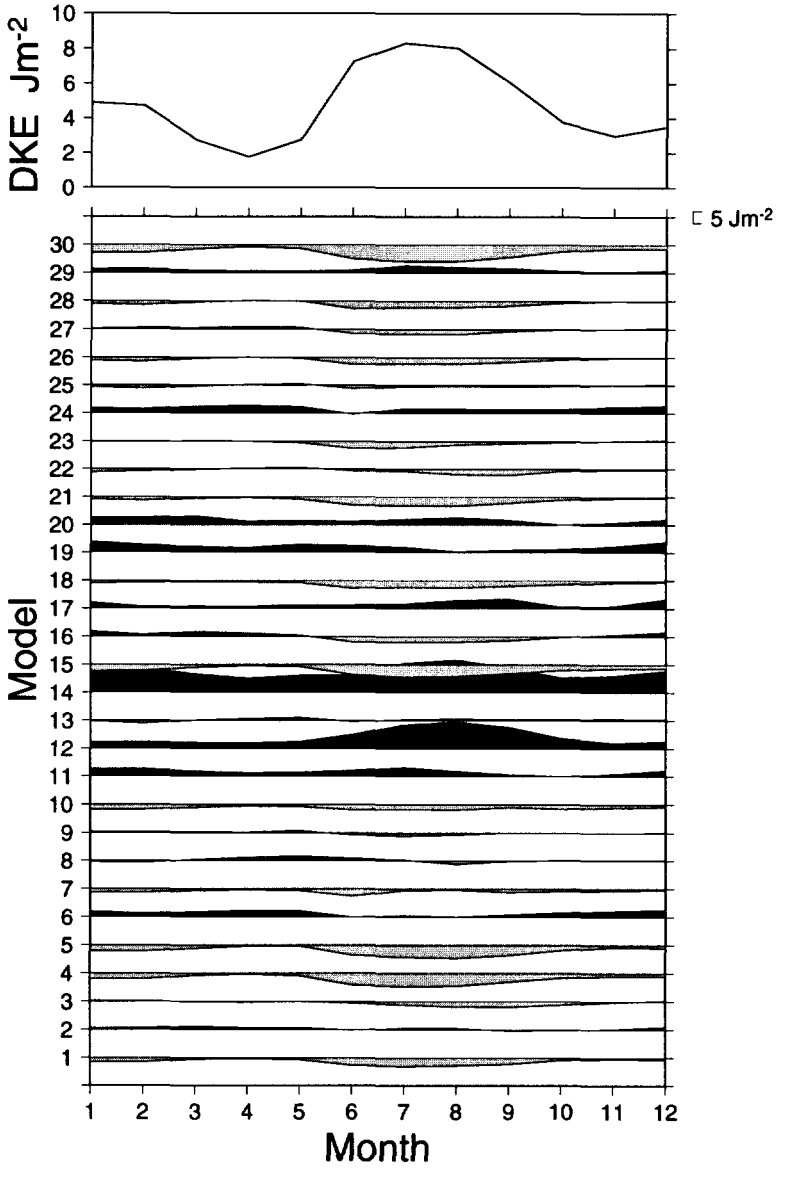

Figure 11. The seasonal cycle of the difference in 200 hPa DKE between the AMIP models and the NCEP / NCAR reanalyses. The dark shading represents an overestimate, the light shading indicates an underestimate by the model. The models are ordered alphabetically (BMRC = 1) as in Table 1. The curve at top are the NCEP / NCAR reanalyses values used in the difference.

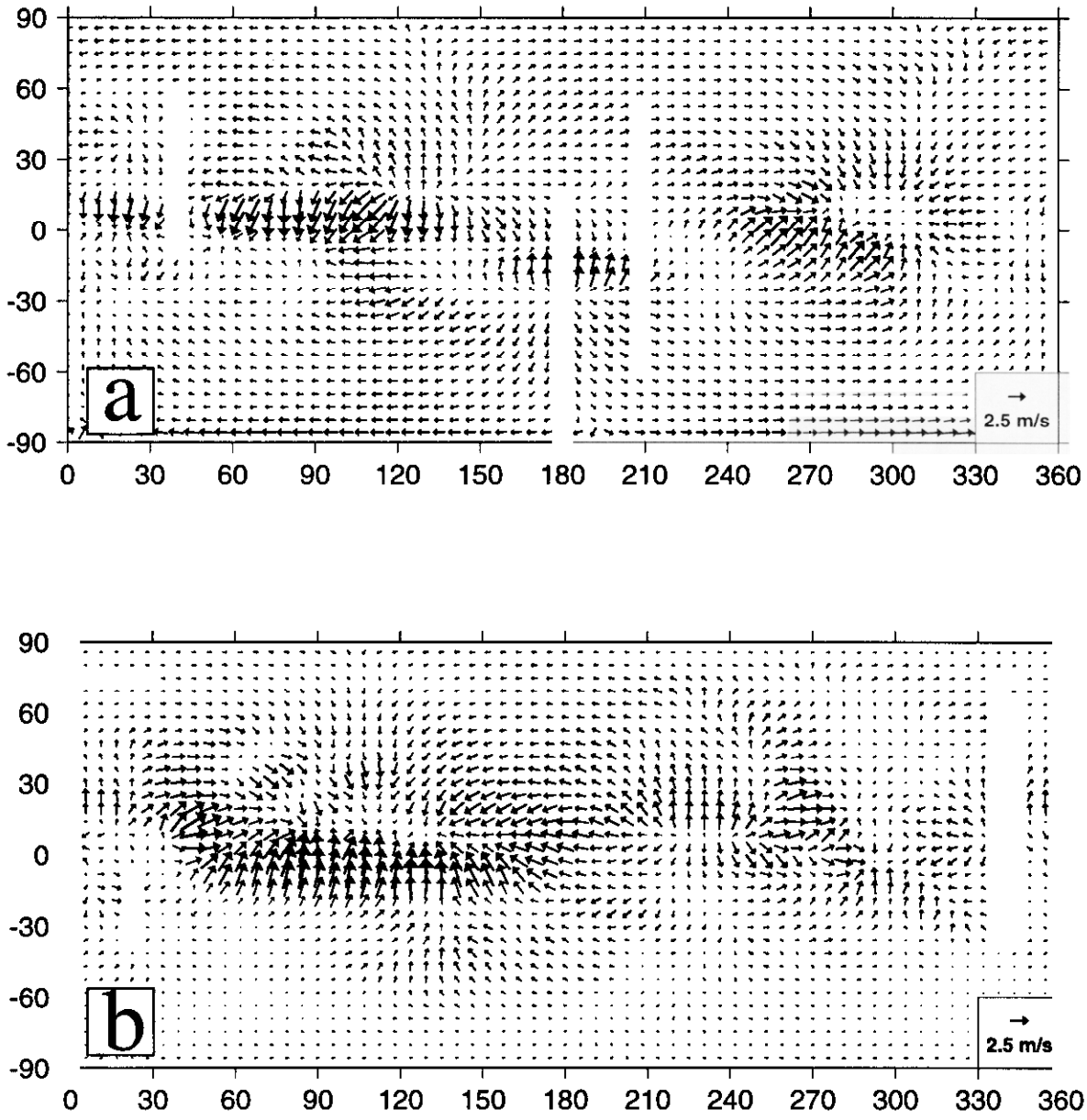

Figure 12. (a) The difference between the divergent wind of the GLA simulation minus the NCEP / NCAR reanalyses, for the northern summer (June, July, August) for the period 1979 to 1988. (b) As in (a) except for the COLA model.

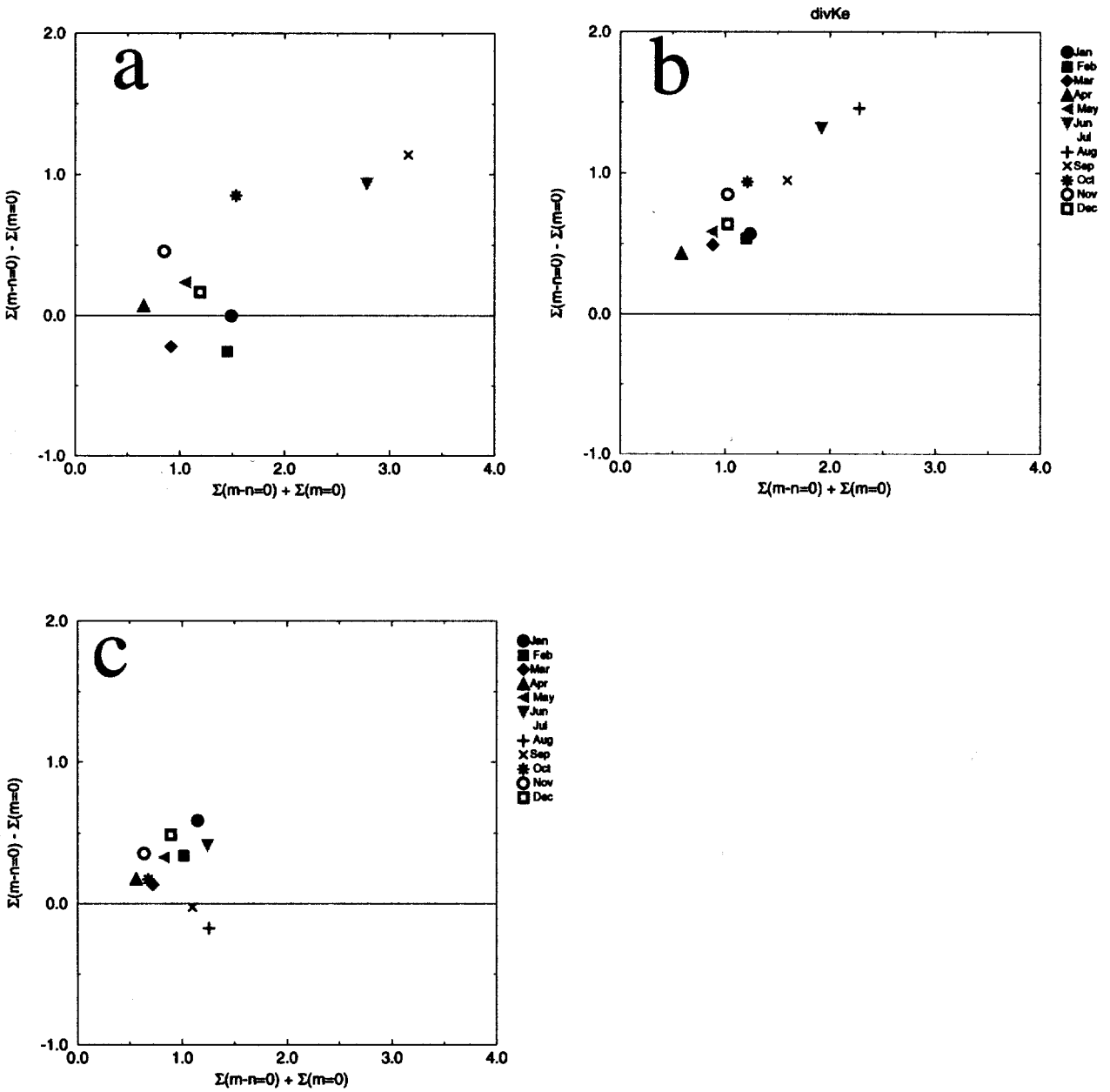

Figure 13 (a) A Tukey sum-difference plot for the Σ(m=0) and Σ(n-m =0) modes of the 200 hPa divergent kinetic energy for the seasonal cycle of the GLA simulation. (b) As in (a) except for the BMRC model. (c) As in (a) except for the COLA simulation.

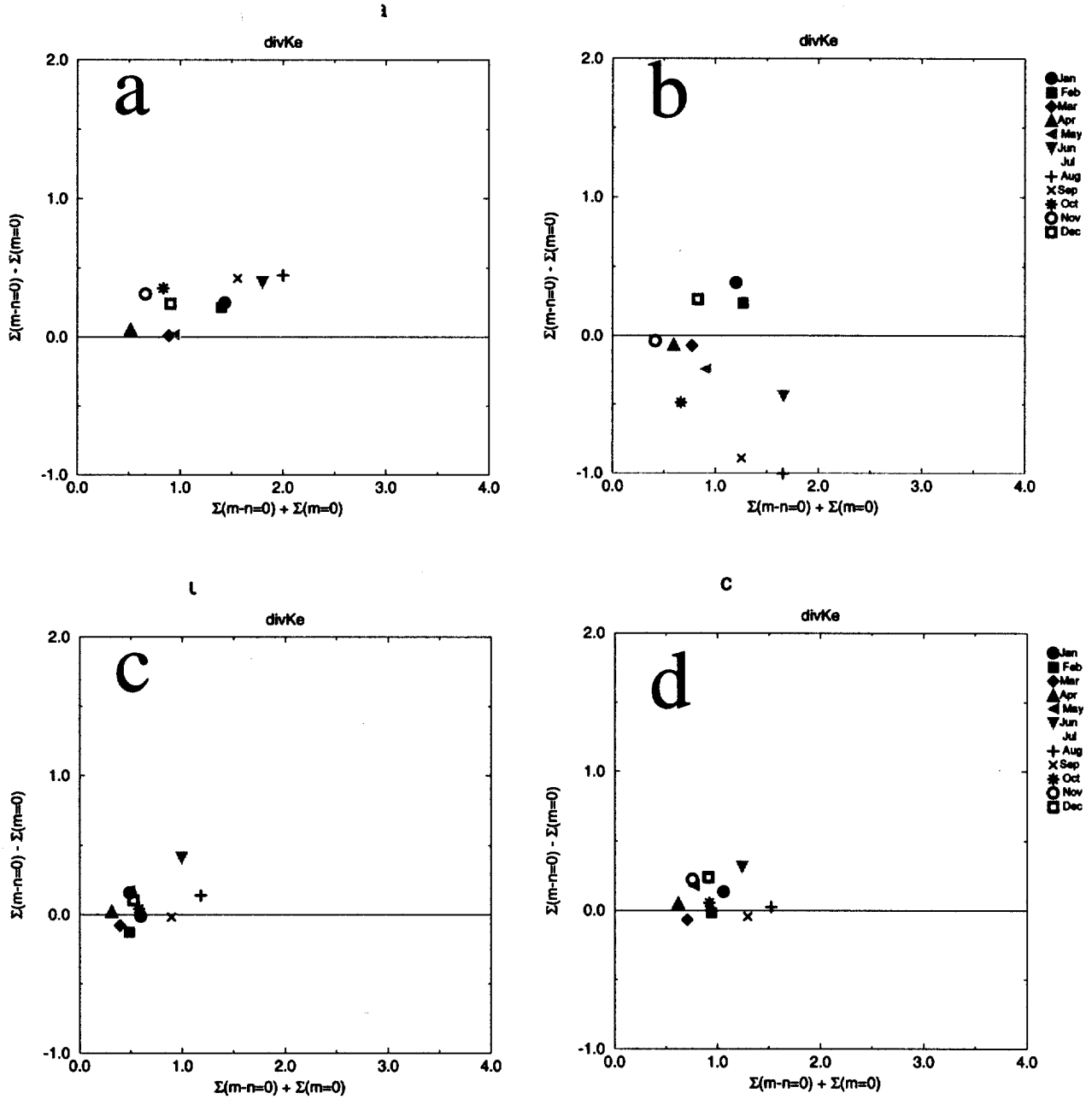

Figure 14 (a) A Tukey sum-difference plot for the Σ(m=0) and Σ(n-m =0) modes of the 200 hPa divergent kinetic energy for the seasonal cycle of the ECMWF simulation. (b) As in (a) except for the UGAMP model. (c) As in (a) except for the UCLA simulation. (d) As in (a) except for the CSU simulation.

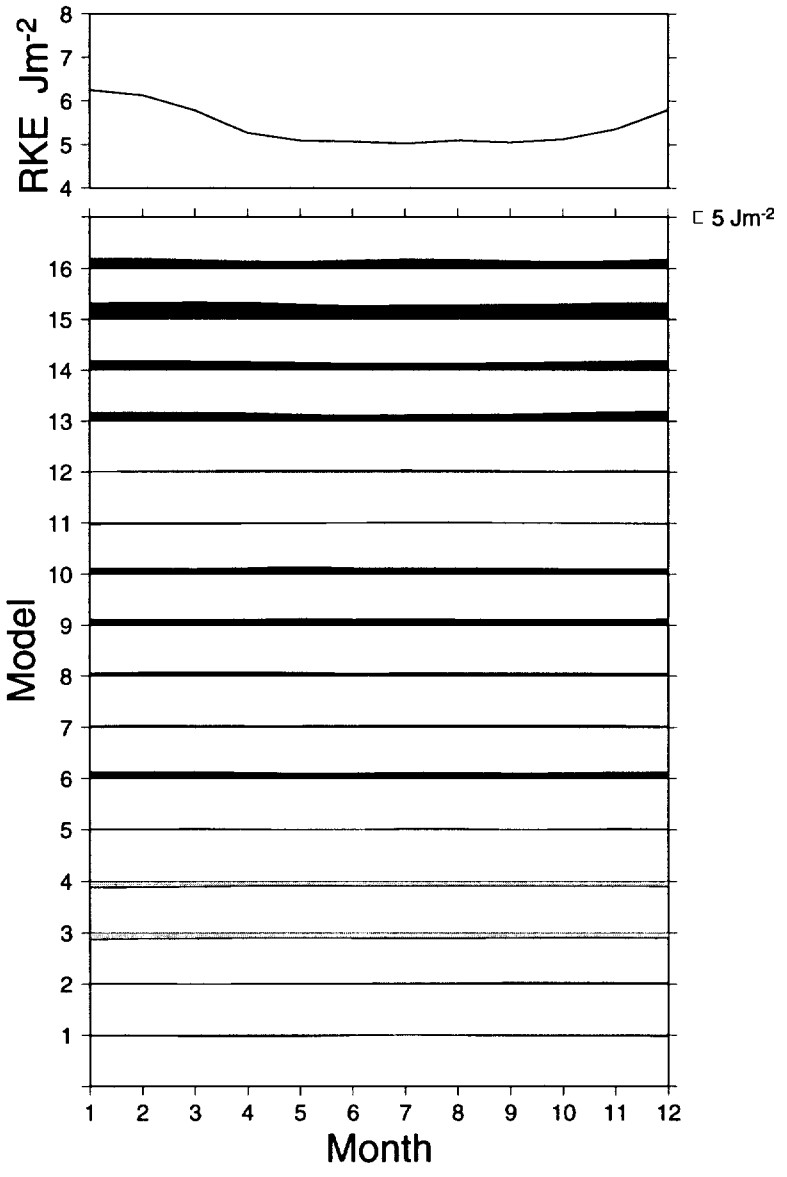

Figure 15. The seasonal cycle in the difference in 200 hPa RKE between some revised AMIP model simulations and the NCEP / NCAR reanalyses. The dark shading represents an overestimate, the light shading indicates an underestimate by the model. The models are ordered as in Table 2 (CNRM = 1,2). The curve at top are the NCEP / NCAR reanalyses values used in the difference.

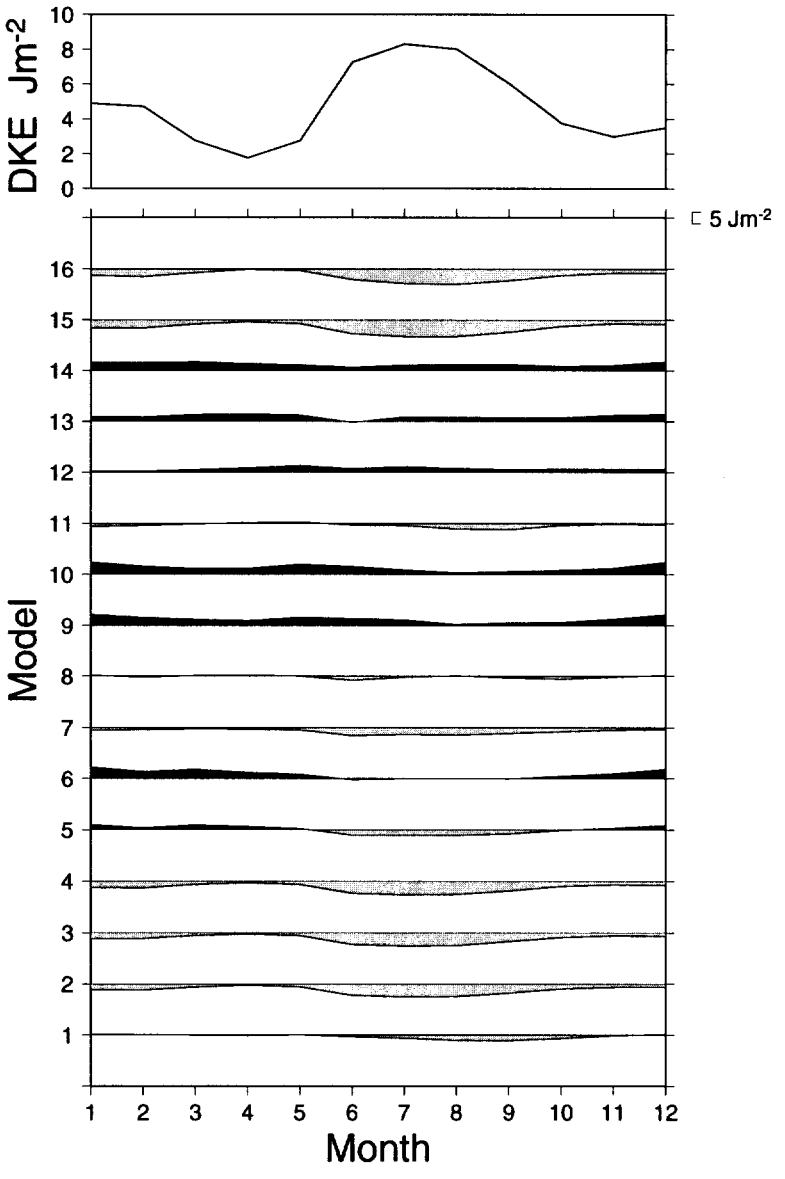

Figure 16. The seasonal cycle in the difference in 200 hPa DKE between some revised AMIP model simulations and the NCEP / NCAR reanalyses. The dark shading represents an overestimate, the light shading indicates an underestimate by the model. The models are ordered as in Table 2 (CNRM = 1,2). The curve at top are the NCEP / NCAR reanalyses values used in the difference.

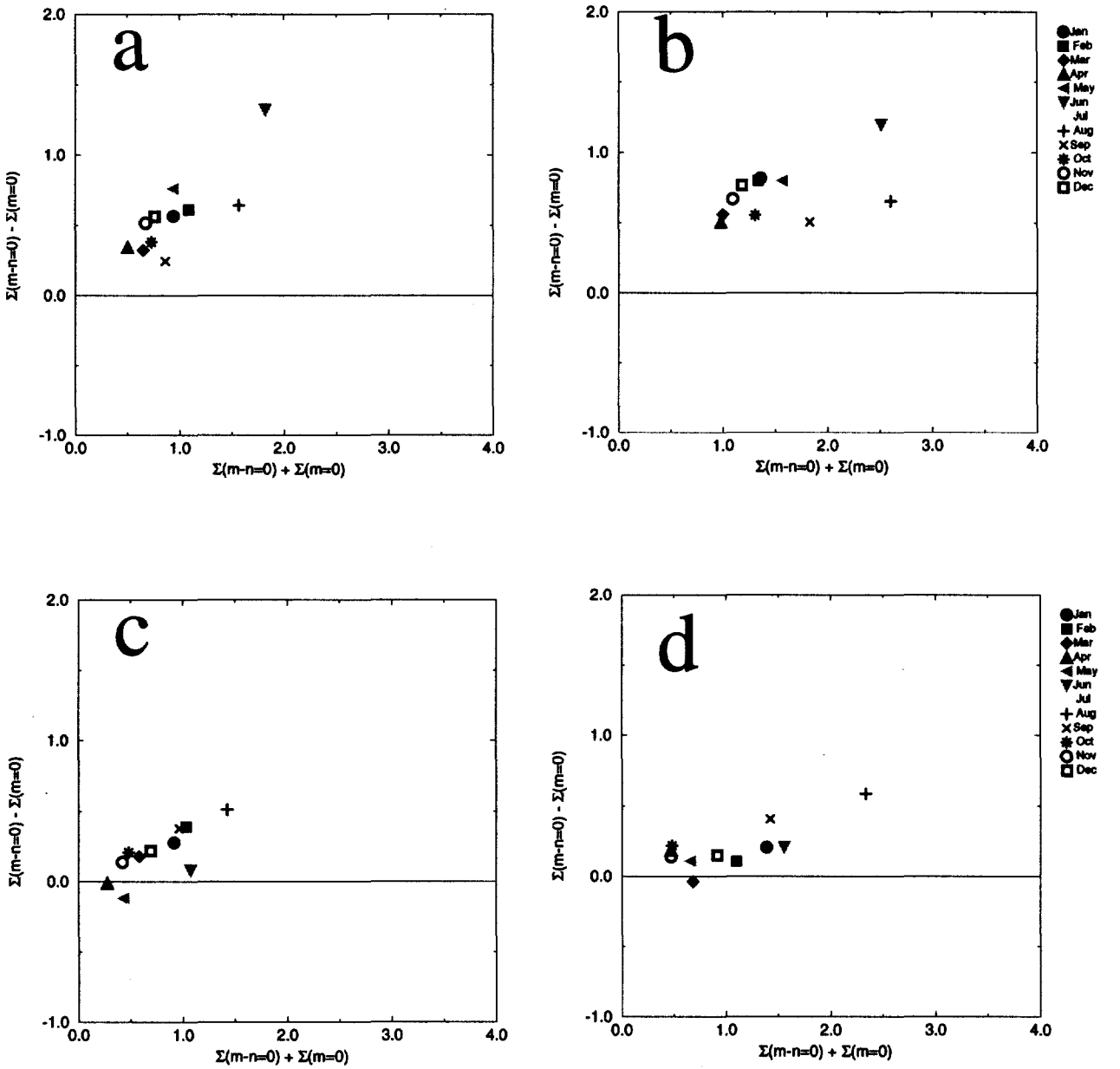

Figure 17 (a) A Tukey sum-difference plot for the $\Sigma(m=0)$ and $\Sigma(n-m=0)$ modes of the 200 hPa divergent kinetic energy for the seasonal cycle of the initial AMIP NRL simulation. (b) As in (a) except for the revised NRL model. (c) As in (a) except for the MPI simulation. (d) As in (a) except for the revised MPI simulation.